JOURNAL OF MATERIALS SCIENCE 20 (1985) 3141 – 3149

# Effect of ribbon–wheel contact on the microstructure of melt-spun Al–Cu eutectic alloy ribbons

W. NEUMANN, M. LEONHARDT, W. LÖSER, R. SELLGER, M. JURISCH
*Central Institute of Solid State Physics and Materials Research of the Academy of Sciences of the GDR, DDR–8027 Dresden, German Democratic Republic*

The microstructure of melt-spun Al–17.3 at % Cu eutectic alloy ribbons with different thicknesses have been revealed by means of electron microscopy and X-ray techniques. Thick ribbons (> 20 $\mu$m) consist of finely-dispersed $\alpha$-Al and $Al_2Cu$ equilibrium phases showing lamellar or irregular morphology. In thin ribbons a considerable fraction of supersaturated $\alpha$-Al solid solution and the metastable $Al_4Cu_9$ phase have been detected. The experimental facts on the identity of the phases, their morphology and particle size for given processing conditions are discussed within the framework of a heat flow model including the solidification process as well as post-solidification transformations. The microstructural features are considered to be determined by local and time variations of the ribbon–wheel contact.

## 1. Introduction

Although the melt-spinning technique is widely used for the production of amorphous and microcrystalline alloy ribbons, the solidification process is not fully understood because of the many influencing factors. On the other hand it is well known that much information concerning the rapid solidification process is available from the microstructural features of rapidly-quenched crystalline foils such as lamellar spacing in eutectic alloys, dendrite arm spacing and extended solid solubility [1, 2].

In particular the microstructure of splat-quenched Al–Cu alloy foils has been investigated extensively [3–6] and several conclusions were drawn on the cooling conditions.

No such investigation for melt-spun ribbons is known except for transmission electron microscopic (TEM) results for some electron-transparent thin regions observed near the centre of the ribbons [7]. These results may not be representative of ribbons with overall thicknesses of 20 to 50 $\mu$m.

The purpose of this paper is a detailed investigation of the microstructure of Al–17.3 at % Cu eutectic alloy ribbons produced by the melt-spinning technique as a function of process parameters. Special care was taken with respect to the influence of the melt–wheel wetting conditions on the local microstructure of the ribbon. The results are discussed in the framework of a solidification model described in a previous paper [8]. This allows some conclusions to be drawn from the observed microstructural features concerning the freezing process.

## 2. Experimental procedures

Pure (99.999%) aluminium and copper were used to prepare the Al–17.3 at % Cu eutectic master alloy. Casting was carried out under 13.3 Pa vacuum. The ribbons were produced by a melt-spinning apparatus of the Liebermann–Graham type [9] with a 160 mm diameter copper roller and a quartz tube with a circular orifice of 0.8 mm diameter. The substrate–orifice distance was about 1 mm. Ribbons of 1 to 5 mm width and 8 to 40 $\mu$m thickness were obtained by varying the linear surface speed and the ejection

0022–2461/85 $03.00 + .12 

pressure within the ranges of 20 to 80 m sec$^{-1}$ and 1.0 × 10$^4$ to 1.5 × 10$^5$ Pa respectively. The morphology of the wheel side of the ribbons, which results from the melt–substrate wetting conditions and depends sensitively on the process parameters [10], was investigated by optical and scanning electron microscopy (SEM).

The microstructure of selected ribbons was characterized by the following methods:

(a) SEM studies of wheel-side, air-side and fracture surfaces of as-cast ribbons;

(b) transmission electron microscopic (TEM) investigation of replicas made from polished and etched ribbon cross-sections; and

(c) X-ray phase analysis and X-ray micro-diffractometer [11] investigations of as-cast and annealed ribbons.

In some cases the temperatures of ribbons after separation from the wheel were measured by a calorimetric method in order to relate the microstructure with some features of the cooling process.

## 3. Results

### 3.1. Morphology of wheel-side surface and fracture surfaces of ribbons

It has been shown that the wetting pattern, which itself depends on several processing conditions such as wheel surface topology and linear surface speed, considerably influences the ribbon–wheel interfacial heat transfer [10]. Therefore it may be expected also to determine the microstructure of the ribbon.

In Fig. 1 typical morphologies of wheel-side surfaces of Al–Cu ribbons are shown in the case of a longitudinally polished wheel surface. For linear surface speeds $v_s < 60$ m sec$^{-1}$ the lift-off areas form channels arranged in a fishbone pattern on the ribbon surface (Fig. 1a). The character of lift-off areas is transformed into single air pockets with further increase in $v_s$ (Fig. 1b). The lift-off area fraction is about 30% of the whole surface. The lift-off morphology on the wheel-side surface is superposed by a coarse network of regions which are lifted off from the substrate although exhibiting the impression of the wheel profile (bright regions in Fig. 1c). A pecularity of these regions are small nearly circular hillocks which are partially flattened on top. Probably these regions originate from an initial melt–wheel contact which was lost in a later stage of the solidification process. The surface fraction of permanent ribbon–wheel contact (dark regions in Fig. 1c), which is about 20% at $v_s$ = 20 m sec$^{-1}$, is increased by increasing $v_s$. At $v_s$ = 80 m sec$^{-1}$ no sign of this network was observed. An air screen behind the melt puddle effectively reduced the lift-off area fraction,

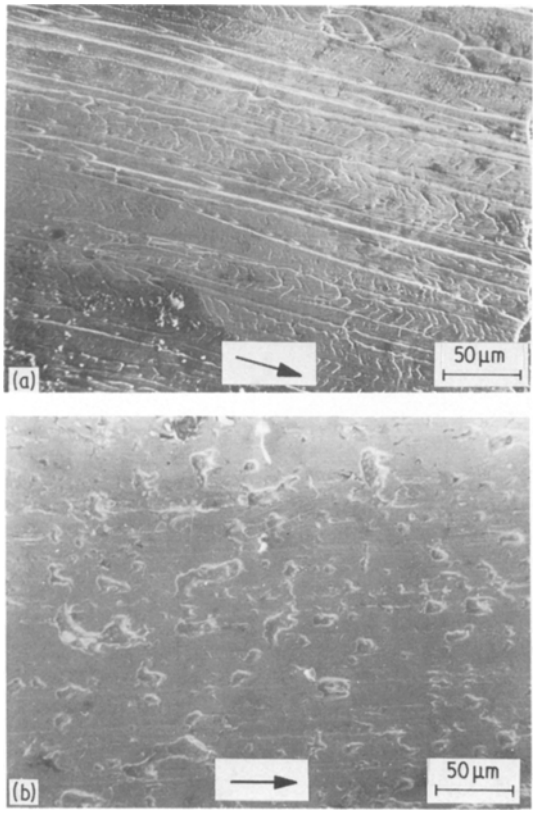


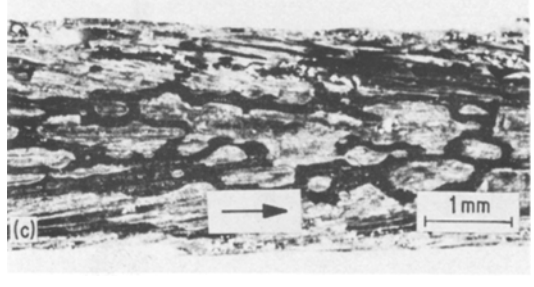


*Figure 1* Wetting pattern at the wheel-side surface of ribbons for different linear surface speeds $v_s$ (the arrows indicates the direction of spinning): (a) SEM micrograph showing channels at $v_s$ = 20 m sec$^{-1}$ ($d \approx 40\,\mu$m); (b) SEM micrograph showing pockets at $v_s$ = 70 m sec$^{-1}$ ($d \approx 15\,\mu$m); (c) optical micrograph showing coarse network at $v_s$ = 50 m sec$^{-1}$ ($d \approx 20\,\mu$m).

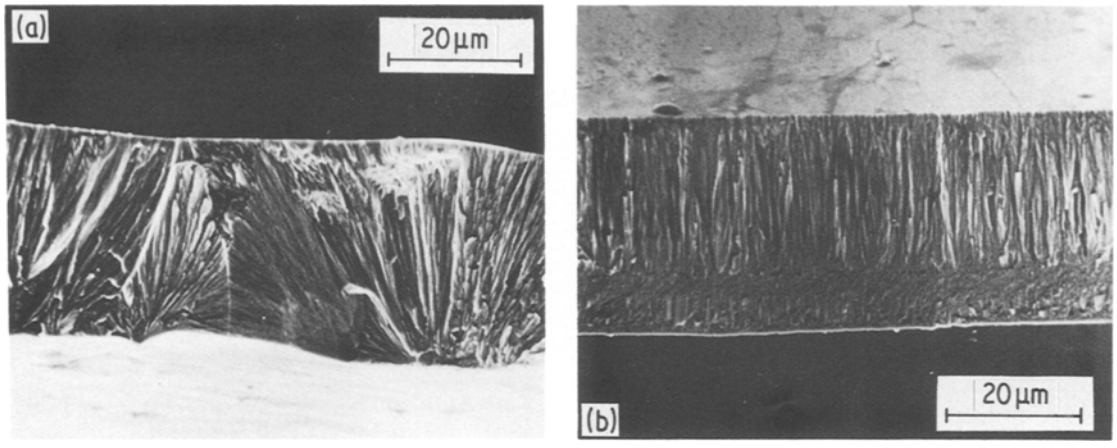


*Figure 2* Optical micrograph showing grain structure on fracture surfaces of ribbon cross-sections (the wheel-side surface is at the bottom): (a) near a localized ribbon–wheel contact area; (b) for more homogeneous ribbon–wheel contact.

giving rise to the presumption that they are mainly formed by air trapping at the back of the melt puddle [10].

The importance of the melt–substrate wetting pattern for the solidification process is demonstrated by some cross-sectional fracture surfaces of ribbons. The main portion of the ribbon, except for a thin layer of globular grains in the immediate vicinity of the wheel-side surface, is occupied by columnar grains (Fig. 2). The columnar grain direction is mainly determined by the heat flow, although an influence of the fluid flow in the melt puddle has been reported to cause an overall inclination of the growth direction of some 10° to the ribbon plane normal [12, 13]. The latter effect is only visible on longitudinal ribbon sections. Therefore the observed spread in the columnar grain inclination on the cross-section of the ribbon (perpendicular to the casting direction) is essentially due to the inhomogeneous thermal contact (Fig. 2a). The columnar grains seem to originate in the contact areas, which is consistent with the heat flow calculated previously [8]. For more homogeneous contact the columnar grains are directed almost parallel to the ribbon plane normal (Fig. 2b).

## 3.2. Microstructure of as-quenched ribbons

In accordance with the observations of other authors [1, 3–6] the local microstructure of rapidly-quenched foils was found to be non-uniform. Two distinct types of microstructures were observed, depending on the ribbon thickness $d$. For $d \gtrsim 20\,\mu m$ (corresponding to $v_s < 50\,m\,sec^{-1}$ at a fixed ejection pressure of $p = 150\,kPa$) the ribbon consists of the equilibrium phases α-Al and $Al_2Cu$ as revealed by X-ray methods. The topology of the microstructure essentially depends on its distance from the ribbon–wheel interface as shown in Fig. 3. Two regions of different topology can be distinguished. A coarse cellular duplex structure with typical particle sizes of 0.1 to 0.15 $\mu m$ is predominant in a layer about 10 $\mu m$ thick at the wheel-side of the ribbon. This region is succeeded by a lamellar eutectic structure with lamellar spacings $\lambda$ varying from about 0.035 $\mu m$ through a maximum of about 0.060 $\mu m$ to again smaller values of about 0.035 $\mu m$ with increasing distance from the wheel-side surface.

This sequence of topology and lamellar spacings was found to be typical for all ribbons investigated, though the values of $\lambda$ depend on ribbon thickness and local scatter within a given ribbon. The different nature of the microstructure of the air-side and the wheel-side of the ribbon exhibiting lamellar eutectic and cellular duplex topology, respectively, is also demonstrated in Fig. 4 (bright regions correspond to the $Al_2Cu$ phase).

Above large lift-off areas, where the heat flow direction is expected to deviate from the ribbon plane normal, coarse lamellae were observed at the wheel-side surface of the ribbon which contrast with the cellular duplex topology on the remaining ribbon surface. The lamellae are directed from the edges to the centre of the lift-off region (Fig. 4c). This would correspond

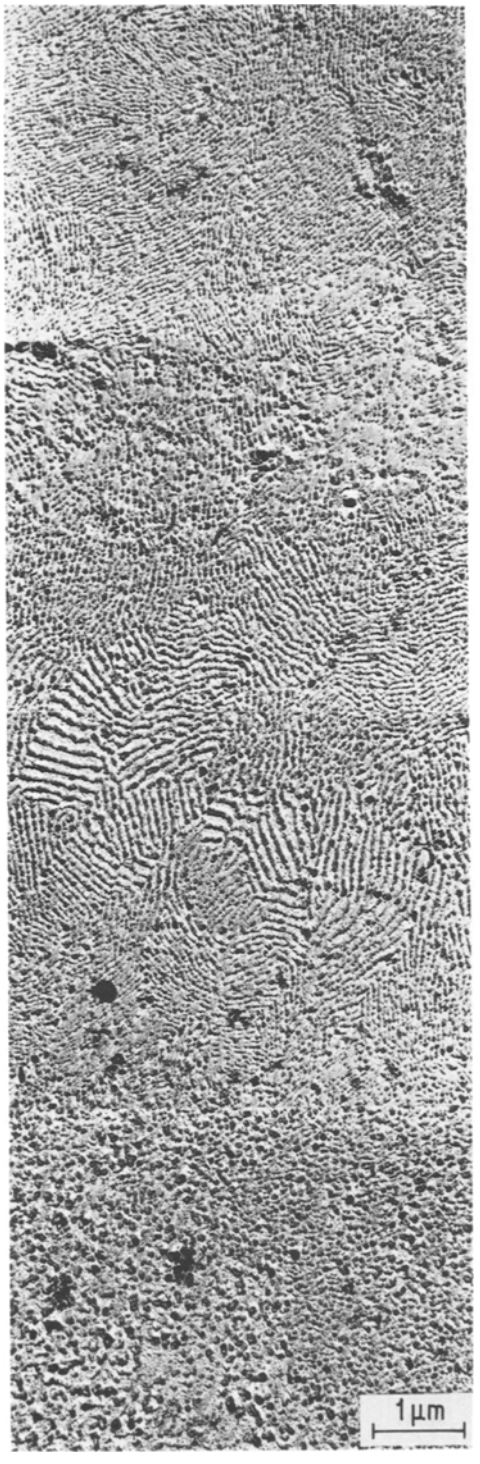


*Figure 3* TEM replica micrograph of a cross-section of a 30 $\mu$m thick ribbon showing the sequence of microstructures through the cross-section. The bottom edge of the micrograph corresponds to a distance of 5 $\mu$m from the wheel-side surface of the ribbon.

to a solidification front velocity which is essentially directed parallel to the ribbon–wheel interface, as is expected when the heat is not directly conducted into the chill block but instead extracted via neighbouring ribbon–wheel contact points [8]. One reason for the decrease of lamellar spacing from the edges to the centre of the lift-off region should be the decreasing ratio of solidifying volume to solidification front area during the solidification of such insulated domains. Another conceivable factor causing the solidification front velocity to increase is the steadily decreasing melt superheat during the solidification process.

In thin ribbons ($d \lesssim 20\,\mu$m) supersaturated $\alpha$-Al solid solution and the metastable vacancy-ordered $Al_4Cu_9$ phase which was previously reported to occur in rapidly-quenched Al–45 at % Cu foils [14] were detected by X-ray diffraction in addition to the equilibrium phases $\alpha$-Al and $Al_2Cu$. Comparing the lattice constant of the supersaturated $\alpha$-Al solid solution $a = 0.397$ nm with that of Predel and Duddek [15] the copper concentration is concluded to be approximately 17 at %, i.e. it corresponds to the eutectic composition of the melt. From the intensity of the corresponding X-ray diffraction lines the volume fractions of supersaturated $\alpha$-Al solid solution and of the metastable $Al_4Cu_9$ phase in an as-quenched ribbon with $d \approx 8\,\mu$m were roughly estimated to be of order of 60% and about 1% respectively. Furthermore, the intensity of the corresponding X-ray diffraction lines of the supersaturated $\alpha$-Al solid solution continuously decreased during a heat treatment of 15 h at 423 K, whereas that of the metastable $Al_4Cu_9$ phase passed through a maximum. This gives rise to the opinion that the $Al_4Cu_9$ phase should be a solid state decomposition product of the highly supersaturated $\alpha$-Al solid solution.

In TEM replica micrographs of the cross-sections of thin ribbons a featureless zone near the wheel-side surface was observed in analogy with that found in rapidly-quenched Al–Si foils [16]. It probably corresponds to the supersaturated $\alpha$-Al phase. Near the air-side surface a fine-grained lamellar structure with the smallest observed value $\lambda \approx 0.016\,\mu$m occured.

The fraction of supersaturated $\alpha$-Al gradually decreases with increasing ribbon thickness. Near $d \approx 20\,\mu$m localized single-phase $\alpha$-Al regions were detected above contact areas by means of

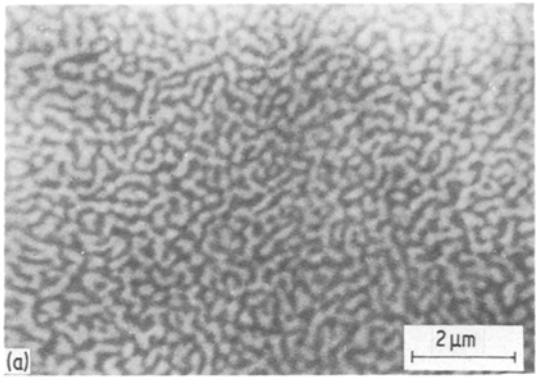


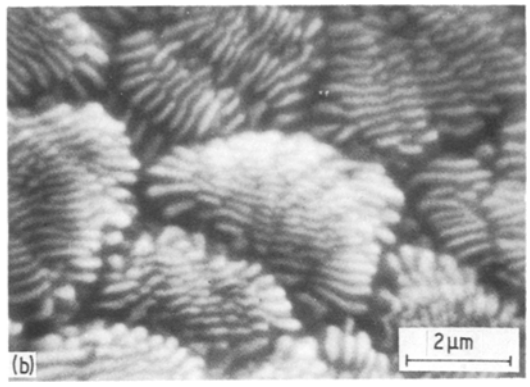


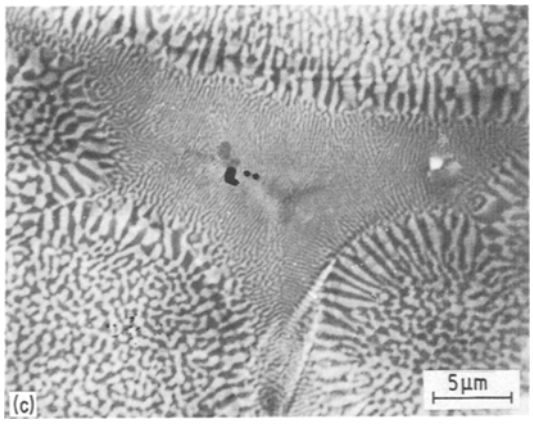


*Figure 4* SEM micrographs of (a) wheel-side surface; (b) air-side surface of a 30 μm thick ribbon; (c) wheel-side surface over a large lift-off area.

X-ray micro-diffractometry [14]. The striking difference between the X-ray diffraction patterns of ribbon sections above a contact area *A* and a lift-off area *B*, which were obtained only in the back scattering direction for technical reasons, is illustrated in Fig. 5. In the diffraction pattern of Section *B* only diffraction lines of the α-Al and $Al_2Cu$ equilibrium phases are obtained. The diffraction pattern of Section *A* essentially contains a very smoothed (3 1 1)–α-Al diffraction line which is considerably shifted toward greater Bragg angles. The maximum intensity corresponds to an average lattice constant of $a = 0.3989$ nm, equivalent to some 13 at % Cu in the supersaturated α-Al solid solution. The considerable line broadening can be related to a spread of the copper concentration of about ±7 at % in the α-Al solid solution. Moreover it can also be caused by the small crystallite sizes.

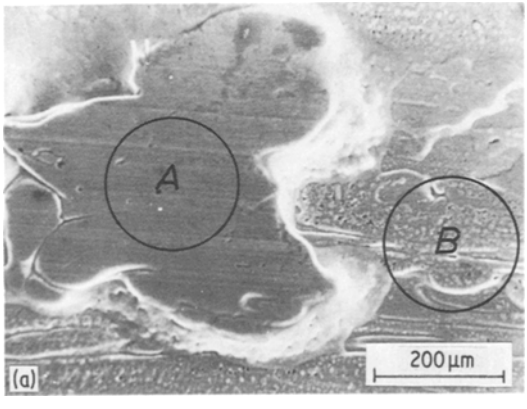


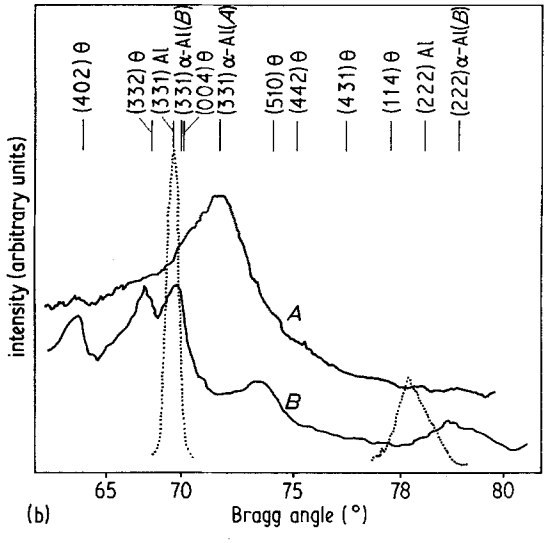


*Figure 5* X-ray micro-diffraction investigation of ribbon sections with different ribbon–wheel contacts ($d \approx 20$ μm): (a) SEM micrograph showing the wheel-side surface of the ribbon with circles indicating the regions investigated over a contact area (*A*) and a lift-off area (*B*); (b) X-ray (Cr-*K*α) diffraction patterns of ribbon sections over the areas *A* and *B* (full lines) and of pure aluminium for comparison (dashed line). Reflex positions of α-Al(Cu) and θ-$Al_2Cu$ are indicated.

## 4. Discussion

According to previous workers [1, 8] the observed microstructure should be either a direct result of the solidification process, of post-solification transformations, or of both. Supposing the fine lamellar microstructure to originate primarily from the solidification process we use the relation $\lambda^2 v = 88.1 \times 10^{-18}\,\mathrm{m^3\,sec^{-1}}$ [1, 3] for the estimation of the solidification front velocity $v$ from the observed lamellar spacing. With $\lambda = 0.035\,\mu\mathrm{m}$ determined near the air-side surface of a 30 $\mu$m thick ribbon (see Fig. 3) one obtains $v = 0.072\,\mathrm{m\,sec^{-1}}$ corresponding to a cooling rate $\dot{T} = 1.0 \times 10^6\,\mathrm{K\,sec^{-1}}$ [3]. This solidification front velocity is compared with the predictions of rapid solidification models [8, 17]. We obtain a ribbon–wheel heat transfer coefficient $h = 1.7 \times 10^5\,\mathrm{W\,m^{-2}\,K^{-1}}$ and a Nusselt number $Nu = 0.062$ ($Nu = hdk_s^{-1}$, where $k_s$ is the thermal conductivity of the solid ribbon). The Nusselt number is almost within the range of Newtonian cooling $Nu < 0.015$ [18]. In that case rapid solidification models predict an almost constant solidification rate throughout the ribbon [8, 17, 18]. Apparently, this contradicts the experimentally observed sequence of lamellar spacings with distance from the wheel-side surface (see Fig. 3). In particular the narrow region of relatively coarse lamellae must be associated with a minimum in the local solidification rate. Such a kind of minimum was predicted to exist by model calculations [8, 17] for $Nu \gtrsim 1$ if superheating [8] or supercooling [17] were taken into account. Both the Nusselt number determined from the experimentally observed lamellar spacings, as well as the expected depth of the minimum, conflict quantitatively with the model conditions.

One way out of these difficulties is to assume a time-dependent heat transfer coefficient during the solidification process [8]. The calculated solidification front velocity of a solidifying melt layer of the Al–17.3 at % Cu eutectic alloy on a copper substrate is illustrated in Fig. 6.

The details of the mathematical model as well as the physical parameters are given elsewhere [8]. The initial temperature of the melt was 200 K above the melting point. As the solidification front reached one third of the foil thickness the foil–substrate heat transfer coefficient was reduced from an initially high value by a factor of 30. Indeed a distinctly marked minimum in the solidification front velocity is predicted in the transient stage after the reduction of heat transfer. This surprising behaviour is explained as follows. Steep temperature gradients exist both in the solidified foil as well as in the remaining melt layer during the first stage of the solidification process, determined by a high heat transfer coefficient. On suddenly reducing the foil–substrate heat transfer the temperature gradient is first decreased in the solidified layer near the substrate, whereas the heat flow from the superheated melt to the liquid–solid interface remains unaffected. The solidification front velocity is therefore decreased. In extreme cases a remelting of the solidified layer may occur [8]. After this transient stage the temperature gradient in the melt gradually attains a smaller value and the solidification front velocity is again increased.

The possibility of an abruptly decreased heat transfer during the solidification process, as a consequence of a partial ribbon–wheel separation, is strongly supported by the existence of the coarse network at the wheel side of the

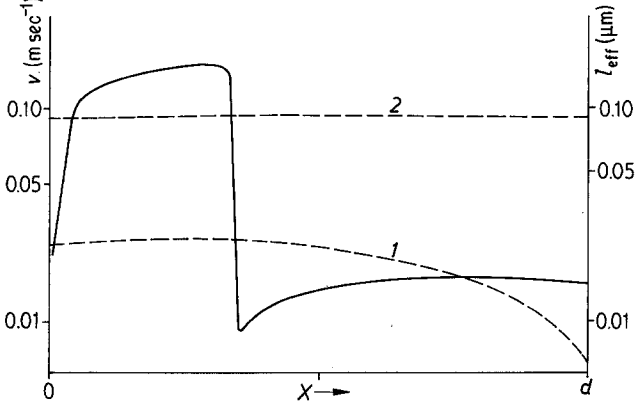


*Figure 6* Predicted local solidification rate $v$ (full line) and effective diffusion length $l_{\mathrm{eff}}$ (dashed line) plotted against ribbon–wheel interfacial distance $X$ of a ribbon with $d = 30$ $\mu$m. The ribbon–wheel interfacial heat transfer coefficient is reduced at $t_1 = 1.05 \times 10^{-4}$ sec from $h_1 = 4.2 \times 10^6\,\mathrm{W\,m^{-2}\,K^{-1}}$ to $h_2 = 1.26 \times 10^5\,\mathrm{W\,m^{-2}\,K^{-1}}$. Effective diffusion length $l_{\mathrm{eff}}$ for two different post-solidification modes: (1) Persisting thermal ribbon–wheel contact ($h_2$), (2) air cooling ($h_3 = 3.5 \times 10^2\,\mathrm{W\,m^{-2}\,s^{-1}}$) of the solidified ribbon for $t > 6.3 \times 10^{-2}$ sec.

ribbon discussed in Section 3.1. The observation of the impression of the wheel profile at lifted-off regions of the ribbon surface leads us to assume that even those regions must have had an intimate substrate contact in an early stage of ribbon formation. The considerable difference between the fine-grained layer adjacent to the wheel-side surface and the columnar grains in the remaining part of the ribbon, known from the fracture surfaces (Fig. 2), may also be due to some sudden transition of the ribbon–wheel interfacial heat transfer.

At first glance the observation of the layer of rather coarse irregular two-phase structure on the bottom side of the ribbon seems to argue against a high solidification front velocity in that region. But it should be considered that this kind of microstructure might originate from solid state transformation in the ribbon during the subsequent cooling process [19]. For high solidification front velocity two types of primary structures could be expected: a very finely spaced eutectic [7] or alternatively a homogeneous supersaturated solid solution [5]. According to Sellger *et al.* [8] we can describe processes like coarsening of eutectic structures or precipitation from a supersaturated solid solution by an effective diffusion length:

$$l_{\text{eff}} = \left[\int_{T_M}^{T_0} D(T)\,\frac{\mathrm{d}T}{\dot{T}}\right]^{1/2}. \qquad (1)$$

An Arrhenius law was assumed for the diffusion coefficient $D(T)$. Results of $l_{\text{eff}}$ are also shown in Fig. 6. The sudden change in heat transfer during the solidification process has no particular influence on this quantity. A rather small $l_{\text{eff}}$ of order 0.01 $\mu$m is predicted if the ribbon–wheel contact persists during the further cooling process of the solidified foil (Line 1 of Fig. 6). If the much slower air cooling dominates after solidification, e.g. because of ribbon–wheel separation, $l_{\text{eff}}$ may be increased by nearly one order of magnitude (Line 2 of Fig. 6).

Air cooling must be taken into account because we determined by calorimetric measurements that the temperature of the ribbons was still between 620 and 720 K after separation from the wheel. Replacing the quantity $D(T)t$ (where $t$ is annealing time) in the well-known formulae for isothermal transformations by $l_{\text{eff}}^2$ leads to the following characteristic size parameters, the lamellar half-spacing [20]

$$\lambda^* = \frac{(C_1 l_{\text{eff}}^2)^{1/3}}{2(\Phi/\lambda)_{\text{crit}}} \qquad (2)$$

and the precipitate radius [24]

$$r = \left\{\beta r_s^3\left[1 - \exp\left(-\frac{2^{3/2}\beta^{1/2} l_{\text{eff}}^3}{r_s^3}\right)\right]\right\}^{1/3} \qquad (3)$$

of the coarsened irregular two-phase structure.

We used $C_1 = 8\pi^3 M\gamma c_{\text{eq}}/(RT_1\varrho) = 2.37 \times 10^{-3}\,\mu$m (molar weight $M = 117.5\,\text{kg kmol}^{-1}$, surface free energy $\gamma = 0.1\,\text{J m}^{-2}$, equilibrium solute concentration $c_{\text{eq}} = 1.7$ at %, universal gas constant $R = 8317\,\text{J kmol}^{-1}\,\text{K}^{-1}$, mean coarsening temperature $T_1 = 773$ K, mass density $\varrho = 3.25 \times 10^3\,\text{kg m}^{-3}$) and $\beta = (c_0 - c_{\text{eq}})/(c_p - c_{\text{eq}}) = 0.5$ (solute concentration $c_0 = 17.3$ at %, solute concentration in the precipitate $c_p = 33.0$ at %) and $(\Phi/\delta)_{\text{crit}} \approx 1$ in the calculations. The latter parameter was calculated by van Suchtelen [20] and depends in general on the mode of coarsening and the volume fraction of the affected phase. All parameters were taken at a fixed temperature, because it can easily be verified that they are much less temperature-dependent than the diffusion coefficient. The results are shown in Fig. 7. Some different values of the mean precipitate spacing $r_s$ were used ($4\pi r_s^3 N_p/3 = 1$. Where $N_p$ is the number of precipitates per unit volume).

Notwithstanding the uncertainties of the models as well as the values used for the parameters it is predicted that the cellular duplex structure with observed mean particle size of approximately 0.15 $\mu$m, which is greater than that of the as-grown eutectic structure, is mainly due to precipitation processes from supersaturated solid solution during the relatively slow air-cooling after the ribbon–wheel separation. Only in that case we get $l_{\text{eff}} \approx 0.1\,\mu$m for reasonable parameters (Fig. 6).

The morphology and the particle size of the cellular duplex structure are nearly identical with that observed after isothermal annealing (600 sec at 300° C) of splat-quenched foils consisting originally of supersaturated solid solution [19]. For those conditions we calculated $l_{\text{eff}} \approx 0.16\,\mu$m.

In thin ribbons the supersaturated solid solution was at least partially conserved. It is probably located near the wheel-side surface. The upper part of the thin ribbons consists of a finely-spaced eutectic microstructure. The

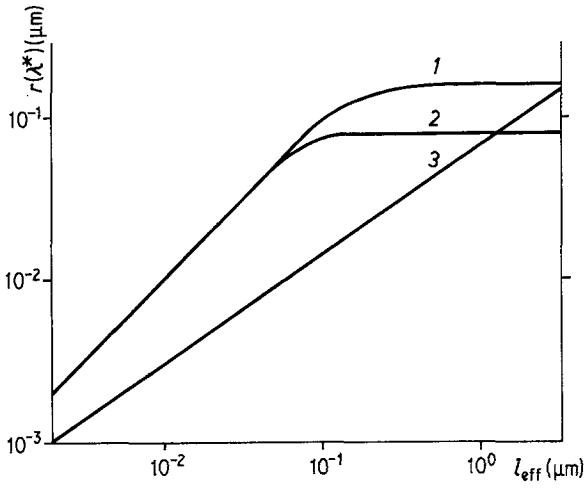


*Figure 7* Particle size $r$ ($\lambda^*$) for different modes of post-solidification transformations plotted against $l_{eff}$. Precipitation from supersaturated solid solution with (1) $r_s = 0.2\,\mu m$, (2) $r_s = 0.1\,\mu m$, (3) coarsening of a eutectic microstructure.

question arises of whether the segregationless solidification in the layer adjacent to the ribbon–wheel interface may be described by a heat flow model where the solidification front velocity is mainly determined by the ribbon–wheel heat transfer, or alternatively occurs unrelated to the external heat extraction because of a prior supercooling of the melt during recalescence from some nucleation temperature well below the melting temperature.

From the dynamic $T_0$-criterion the critical solidification front velocity and supercooling to achieve segregationless solidification of an Al–18 at % Cu alloy were predicted to be $v_c = 0.052\,m\,sec^{-1}$ and $\Delta T_c = 27.6\,K$, respectively [21]. These values seem to be more realistic than those estimated from the Mullins–Sekerka absolute stability criterion (see [2]) which leads, for example, to a one order of magnitude greater value of $v_c$ [21]. It has been suggested that complete rapid solidification during recalescence may occur without external heat extraction if the prior supercooling is at least $L/c$ ($L$ = latent heat of fusion, $c$ = specific heat capacity of the melt) [22]. Lower supercoolings allow only a portion of solidification to occur during recalescence, the remainder occurring at a rate determined by external heat extraction.

Comparing the ratio $L/c$, which amounts to some 440 K for the Al–Cu eutectic alloy with the predicted $\Delta T_c$ necessary for achieving segregationless solidification, we suppose solidification during recalescence to be of minor importance, i.e. the solidification process is essentially determined by external heat extraction as was presumed to be the case in our heat flow model [8]. With the solidification front velocity $v = 0.34\,m\,sec^{-1}$ determined from the smallest observed lamellar spacing $\lambda = 0.016\,\mu m$ we obtained a heat transfer coefficient $h = 8.5 \times 10^5\,W\,m^{-2}\,K^{-1}$ and $Nu = 0.053$ ($d = 8\,\mu m$). These values are considered to be lower limits of the solidification process in thin ribbons and in the layer adjacent to the ribbon–wheel interface of thick ribbons, respectively.

Although the effective ribbon–wheel interfacial heat transfer coefficient was shown to increase with increasing substrate velocity [23], this increment can hardly explain the drastic differences between thick and thin ribbons because the solidification front velocity is only proportional to $h$ and virtually independent of the ribbon thickness. The differences rather occur because of the post-solidification transformations. Calculations performed with the same parameters used for Fig. 6, but with an uninterrupted good thermal contact ($h_1$) until $t_2$ for a 10 $\mu m$ thick ribbon, result in $l_{eff} = 2.42 \times 10^{-3}\,\mu m$. This value of $l_{eff}$ is nearly of the order of the atomic distance. Hence we expect no precipitation in that case. The importance of an uninterrupted thermal contact for maintaining the as-solidified microstructure was also emphasized by the detection of localized sections of supersaturated solid solution surrounded by coarse two-phase microstructure in ribbons of medium thickness (up to 22 $\mu m$). The wheel-side surface in those regions exhibited the impression wheel profile with no sign of lifting off from the wheel.

## 5. Conclusions

Comparing our experimental results on the microstructure of melt-spun Al–17.3 at % Cu eutectic alloy ribbons with theoretical predictions from a heat flow model, we conclude that:

(a) During a first period of the solidification process there exists an intimate contact between ribbon and substrate interrupted on a micrometre scale only by air pockets. A layer of up to 10 $\mu$m is formed consisting mainly of supersaturated solid solution. This structure is preserved down to room temperature if the overall thickness of the ribbon is in the same range.

(b) In a second period of ribbon formation leading to thicker ribbons the heat transfer to the substrate is abruptly decreased in larger regions. Because of the resulting reduced solidification, front velocity-coupled eutectic growth becomes possible. The interlamellar spacing and the growth morphology are a direct measure of the local solidification front velocity. The already-solidified layer is partly re-melted and heat treated, resulting in the observed irregular precipitation structure on the wheel side. The eutectic structure is only slightly modified during cooling down.

These general conclusions should be helpful for an understanding of the solidification process and properties of other microcrystalline or amorphous ribbons as well.


## Acknowledgements

The authors are indebted to Drs J. Henke and D. Stephan for performing the X-ray investigations, and to Professor J. Barthel for helpful discussions.


## References


1. H. JONES, in "Ultrarapid Quenching of Liquid Alloys", edited by H. Hermann (Academic Press, New York 1981) p. 1.
2. *Idem*, in "Rapidly Solidified Amorphous and Crystalline Alloys", edited by B. H. Kear, B. C. Giessen and M. Cohen, (Elsevier, New York, 1982) p. 71.
3. M. H. BURDEN and H. JONES, *J. Inst. Metals* **98** (1970) 249.
4. M. G. SCOTT, *J. Mater. Sci.* **9** (1974) 1372.
5. D. B. WILLIAMS and J. W. EDINGTON, *ibid.* **12** (1977) 126.
6. R. K. SINGH, K. CHATTOPADHYAY, S. LELE and T. R. ANANTHARAMAN, *ibid.* **17** (1982) 1617.
7. K. CHATTOPADHYAY, A. P. RAMIENI and P. RAMACHANDRARAO, *ibid.* **15** (1980) 797.
8. R. SELLGER, W. LÖSER and W. NEUMANN, *ibid.* **19** (1984) 2145.
9. H. H. LIEBERMANN and C. D. GRAHAM, Jr., *IEEE Trans. Magn.* **MAG-12** (1976) 921.
10. S. C. HUANG and H. C. FIELDLER, *Metall. Trans.* **12A** (1981) 1107.
11. D. STEPHAN and K. RICHTER, *Cryst. Res. Techn.* **16** (1981) K57.
12. S. C. HUANG and A. M. RITTER, Technical Information Series Report 83CRD 015 (General Electric Corporate Research and Development, Schenectady, 1983).
13. M. J. TENWICK and H. A. DAVIES, *Mater. Sci. Eng.* **63** (1984) L1.
14. G. V. S. SASTRY, K. K. BARIAR, K. CHATTOPADHYAY and P. RAMACHANDRARAO, *Z. Metallkde.* **71** (1980) 756.
15. B. PREDEL and G. DUDDEK, *ibid.* **69** (1978) 773.
16. J. A. VAN DER HOEVEN, P. VAN MOURIK and E. J. MITTEMEYER, *J. Mater. Sci. Lett.* **2** (1983) 158.
17. P. H. SHINGU and R. OZAKI, *Metall. Trans.* **6A** (1975) 33.
18. R. C. RUHL, *Mater. Sci. Eng.* **1** (1967) 313.
19. M. G. SCOTT and J. A. LEAKE, *Acta Metall.* **23** (1975) 503.
20. J. VAN SUCHTELEN, *J. Cryst. Growth* **43** (1978) 28.
21. L. KATGERMAN, *Scripta Metall.* **17** (1983) 537.
22. M. COHEN *et al.*, in "Rapid Solidification Processing: Principles and Technologies II", edited by R. Mehrbian *et al.* (Claitor's, Baton Rouge, 1980) p. 1.
23. S. C. HUANG and H. C. FIEDLER, *Mater. Sci. Eng.* **51** (1981) 39.
24. F. S. HAM, *J. Phys. Chem. Solids* **6** (1958) 335.



*Received 21 March*
*and accepted 15 October 1984*